Modern Physics Letters B
Vol. 28, No. 10 (2014) 1450077 (12 pages)

DOI: 10.1142/S0217984914500778

First-principles study of electronic, optical and thermoelectric properties in cubic perovskite materials $AgMO_3$ (M = V, Nb, Ta)

Asif Mahmood*,‖, Shahid M. Ramay†, Hafiz Muhammad Rafique‡, Yousef Al-Zaghayer*,§ and Salah Ud-Din Khan¶

*Department of Chemical Engineering, College of Engineering, King Saud University, P. O. Box 800, Riyadh 11421, Saudi Arabia
†Department of Physics and Astronomy, College of Science, King Saud University, P. O. Box 800, Riyadh 11421, Saudi Arabia
‡Department of Physics, University of the Punjab, Lahore, Pakistan
§Industrial Catalysts Research, King Saud University, Riyadh 11421, Saudi Arabia
¶Sustainable Energy Technologies Center, King Saud University, Riyadh 11421, Saudi Arabia
‖ahayat@ksu.edu.sa

Received 9 January 2014
Revised 16 February 2014
Accepted 19 March 2014
Published 6 May 2014

In this paper, first-principles calculations of structural, electronic, optical and thermoelectric properties of $AgMO_3$ (M = V, Nb and Ta) have been carried out using full potential linearized augmented plane wave plus local orbitals method (FP − LAPW + lo) and BoltzTraP code within the framework of density functional theory (DFT). The calculated structural parameters are found to agree well with the experimental data, while the electronic band structure indicates that $AgNbO_3$ and $AgTaO_3$ are semiconductors with indirect bandgaps of 1.60 eV and 1.64 eV, respectively, between the occupied O $2p$ and unoccupied d states of Nb and Ta. On the other hand, $AgVO_3$ is found metallic due to the overlapping behavior of states across the Fermi level. Furthermore, optical properties, such as dielectric function, absorption coefficient, optical reflectivity, refractive index and extinction coefficient of $AgNbO_3$ and $AgTaO_3$, are calculated for incident photon energy up to 50 eV. Finally, we calculate thermo power for $AgNbO_3$ and $AgTaO_3$ at fixed doping 10^{19} cm^{-3}. Electron doped thermo power of $AgNbO_3$ shows significant increase over $AgTaO_3$ with temperature.

Keywords: Cubic perovskite; thermoelectric properties; electronic properties; optical properties.

‖Corresponding author.

1. Introduction

$AgMO_3$ ferroelectric perovskite family, where M (Nb, Ta and V) is penta or tetravalent metal cation, reveals a wide range of interesting microwave dielectric properties.[1] Silver-based perovskite niobates, tantalite's and vanadate are ideal compounds for technological applications in telecommunications, optoelectronics, photocatalysis, electrochemical response and rechargeable lithium batteries.[2–4] The study of these materials has suffered due to the synthesis complications resulting from the thermal instability of Ag^+ ions at high temperature. High sintering temperature is required for $AgTaO_3$, while different combination of electrical and mechanical properties can be achieved from $AgNbO_3$ and similar compounds.[5–8] Silver vanadates are used as cathode materials in the lithium ion batteries due to its significant ionic properties. The structural and phase analysis of $AgVO_3$, $Ag_xV_2O_5$ and $Ag_2V_2O_{11}$ has been performed and the three polymorphs of $AgVO_3$: α, β and γ are discovered, while further studies are underway to find the structural chemistry of these phases.[9,10] Furthermore, $AgTaO_3$ and $AgNbO_3$ have a paraelectric phase with cubic symmetry for temperatures above 758 K and 903 K, respectively. A series of structural phase transitions are observed in $AgNbO_3$ with the decrease in temperature that shows its suitability for piezoelectric material.[11–15] Instead of previously studied perovskite with large bandgap, $AgVO_3$, $AgTaO_3$ and $AgNbO_3$ could be the potential candidates for optoelectronic and thermoelectric devices, where semiconductor with small bandgap and optimum carrier concentration of the order of 10^{19} cm^{-3} were key requirement for good candidate.

First-principles calculations offer the most powerful theoretical tool for the studies of electronic, structure and optical properties of solid state materials. These calculations have been performed for these ferroelectric perovskite compounds using pseudopotential method.[16–19] In the present work, however, we have employed the (FP-LAPW + lo) method to calculate structural, electronic, optical and thermoelectric properties of $AgMO_3$ (M = V, Nb and Ta) in the paraelectric phase based on DFT as implemented in the WIEN2K software.[20] This is well established and produces number of results with good agreement with the experiments.[21–27]

2. Calculation Method

For the density functional calculation of the structural, electronic, optical and thermoelectric properties of $AgMO_3$ (M = V, Nb and Ta), Kohn–Sham equations have been solved self-consistently, wherein use of generalized gradient approximation (GGA) put forward by Wu and Cohen[28] has been made to calculate the contribution of exchange and correlation potentials. The crystal structure of $AgMO_3$ (M = V, Nb and Ta) in the paraelectric phase for which these properties have been calculated, is cubic and belongs to space group Pm-3m (No. 221). In the unit cell, there are five atoms of three types (Fig. 1: Ag is located at the origin $(0, 0, 0)$, M is at the central position $(0.5, 0.5, 0.5)$ and the three O atoms are at $(0.5, 0.5, 0.0)$, $(0.5, 0.0, 0.5)$ and $(0.0, 0.5, 0.5)$.

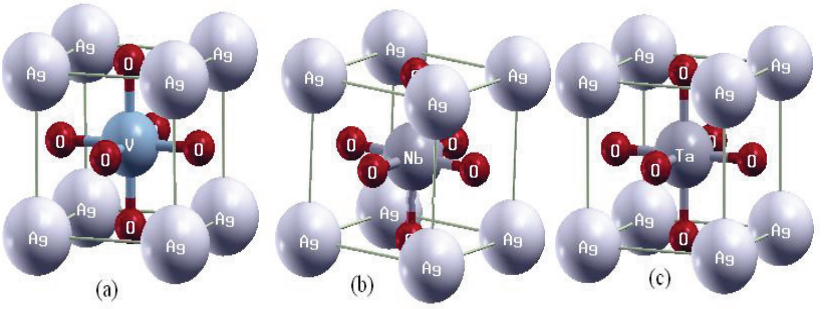

Fig. 1. Crystal structures of cubic perovskite (a) $AgVO_3$, (b) $AgNbO_3$ and (c) $AgTaO_3$.

A muffin–tin (MT) model for the crystal potential has been assumed and the radii R_{MT} for Ag, Nb, Ta, V and O were taken to be 2.5, 1.95, 1.95, 1.95 and 1.73 a.u., respectively. The plane-wave cut-off value of $K_{MAX} \times R_{MT} = 8$ has been used to control the size of basis set for wave functions. The integral over the $10 \times 10 \times 10$ mesh is calculated up to 35 k-points in the irreducible wedge of the BZ. For calculating the optical properties, however, a denser sampling of the BZ is required and a mesh of 120 k-points has been used for these calculations.

3. Results and Discussion

3.1. *Structural properties*

To start with the structural properties, we first calculate the total energy as a function of the unit-cell volume around the equilibrium cell volume by fitting the total energy to the Murnaghan equation of state[29] to calculate the structural parameters of the cubic $AgMO_3$ (M = V, Ta, Nb). Values of experimental lattice constants are used as starting input for $AgTaO_3$ and $AgNbO_3$, while the lattice constants for $AgVO_3$ in paraelectric phase are assumes, and the total energy is minimized with respect to the unit cell volume. The calculated total energies plotted as a function of unit cell volume for compounds are shown in Fig. 2. Calculated equilibrium lattice constants, bulk moduli and derivative of bulk moduli of $AgMO_3$ (M = V, Ta, Nb) are presented in Table 1, and are found to be in good agreement with the experimental results and other theoretical calculations.

3.2. *Electronic properties*

The electronic band structures for $AgMO_3$ (M = V, Ta, Nb) along high symmetry directions are calculated at the symmetry points and along the symmetry line of the Brillouin zone (BZ). Whereas, in case of $AgVO_3$, the conduction and valence bands overlap [Fig. 3(a)] exhibiting the metallic character of this compound. The band structure of $AgTaO_3$ and $AgNbO_3$ presented in Figs. 3(b) and 3(c), respectively shows that the valence band maximum (VBM) lies at M point and the conduction

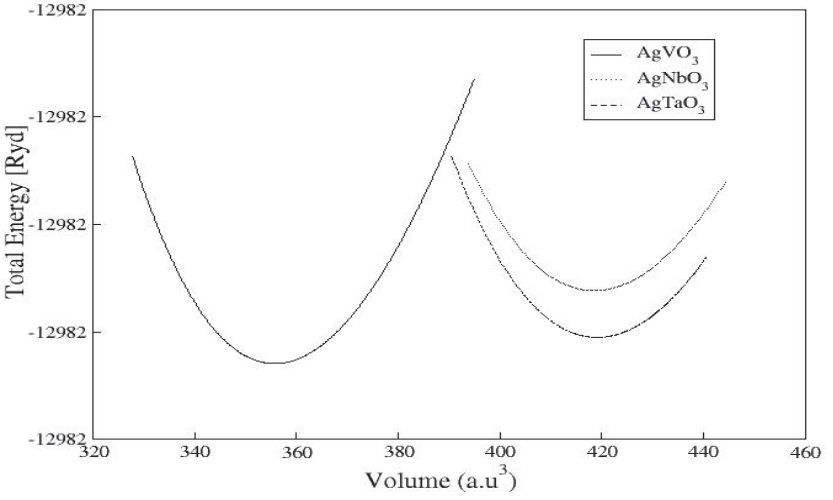

Fig. 2. Total energy as a function of volume for $AgVO_3$, $AgNbO_3$ and $AgTaO_3$.

Table 1. Calculated lattice parameter a_0, bulk moduli **B** and its pressure derivative $\mathbf{B}'$ for $AgMO_3$ (M = V, Nb, Ta) at equilibrium volume compared to other results.

$AgMO_3$ (M = V, Nb, Ta)		WC-GGA	Experimental work	Other theoretical work
$AgVO_3$	a_0 (Å)	3.752		
	B (GPa)	219.35		
	B	4.86		
$AgNbO_3$	a_0 (Å)	3.951	3.9598[a]	3.95[c], 3.79[b]
	B (GPa)	210.37		
	B	5.00		
$AgTaO_3$	a_0 (Å)	3.9588	3.9484[b]	3.95[c]
	B(GPa)	219.76		
	B	5.00		

[a]Ref. 11, [b]Ref. 12, [c]Ref. 16, [d]Ref. 35.

band minimum (CBM) at Γ point for both of these compounds. It clearly indicates that both these compounds are indirect bandgap semiconductors with bandgaps values of 1.60 eV and 1.64 eV, respectively. Our calculated bandgap values are larger than the theoretical calculations done by pseudopotential method,[16] but smaller than experimental values which is 2.8 eV for $AgNbO_3$ and 3.4 eV for $AgTaO_3$.[30] It is well known that density functional calculations underestimate the bandgap values in semiconductors due to the self-interaction error and the absence of derivative discontinuity in the exchange-correlation potential.

The calculated total density of states (DOS) for Ag, V, Nb, Ta and O are shown in Fig. 4. In the valence band of $AgNbO_3$, the energy region [−5.79 eV to 0.1 eV] is

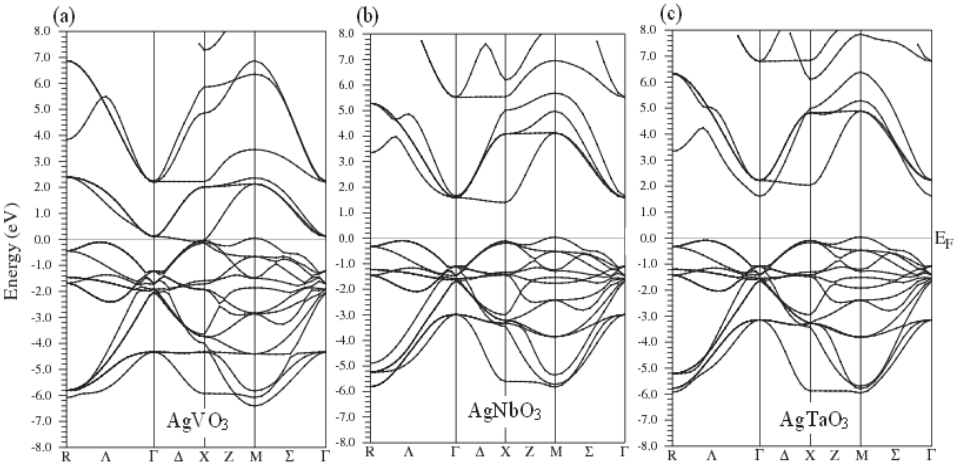

Fig. 3. Calculated band structures of cubic perovskite (a) $AgVO_3$, (b) $AgNbO_3$ and (c) $AgTaO_3$.

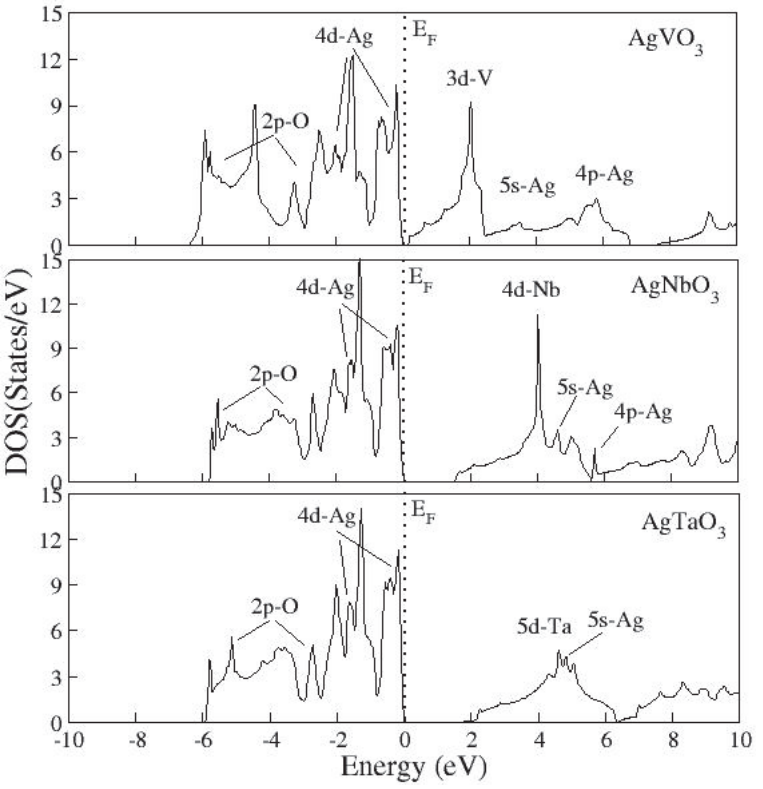

Fig. 4. The calculated TDOS for $AgVO_3$, $AgNbO_3$ and $AgTaO_3$. The energy is with respect to E_F.

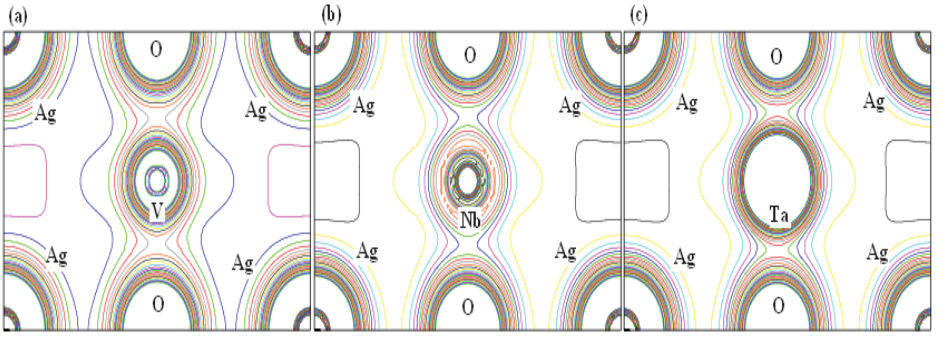

Fig. 5. Contour plots of the valance charge distribution for (a) $AgVO_3$, (b) $AgNbO_3$ and (c) $AgTaO_3$ in the (1 1 0) plane.

mainly occupied by O $2p$ states, indicating strong hybridization with Ag $4d$ states. The conduction band region of $AgNbO_3$ [1.67 eV to 6.01 eV] is dominated by Nb $4d$ states with small contribution of Ag $5s$ and Ag $4p$ states. Therefore, the $4d$ states of Nb and $2p$ states of O are important in the understanding of the electronic properties of $AgNbO_3$. Almost similar behavior with some difference in details is also observed for $AgTaO_3$ and $AgVO_3$.

For $AgMO_3$ (M = V, Nb and Ta), the contour plots of valence charge distribution have been calculated by considering the nature of the corresponding Ag–O, V–O, Nb–O and Ta–O bonds, which are depicted in the (1 1 0) plane. From Figs. 5(a)–5(c), the given plots show a strong ionic but week covalent character of Ag–O bond that can be attributed to the larger charge transfer among Ag and O atoms with very small contour extension. Figure 5(a) reveal the strong sharing and distribution of electrons along the V–O bond. As a result, their bond is strongly covalent with a bond length 1.87 Å. Similarly, strongly covalent nature with a bond length 1.97 Å and 1.98 Å are observed along the Nb–O and Ta–O bond. Due to the metallic nature of $AgVO_3$, it is useless to consider as candidate for optoelectronic devices and due to very small Seebeck coefficient (in metal order of 0.00001 V/K), it could not enhance the thermoelectric properties. Hence, in further study of optical and thermoelectric properties, we exclude $AgVO_3$.

3.3. *Optical properties*

The study of optical properties of these materials provides useful information regarding their application in the opto-electronic devices. We have calculated the frequency-dependent dielectric function $\varepsilon(\omega) = \varepsilon_1(\omega) + i\varepsilon_2(\omega)$ in order to describe the optical properties of $AgTaO_3$ and $AgNbO_3$. In the present calculations, the equation for the frequency-dependent imaginary part of a dielectric function $\varepsilon_2(\omega)$ for cubic crystal has been taken as[31] and it is strongly correlated to the joint density of states and momentum matrix elements. The real part of the dielectric function $\varepsilon_1(\omega)$ can be obtained from $\varepsilon_2(\omega)$ by using Kramers–Krönig relation.[32]

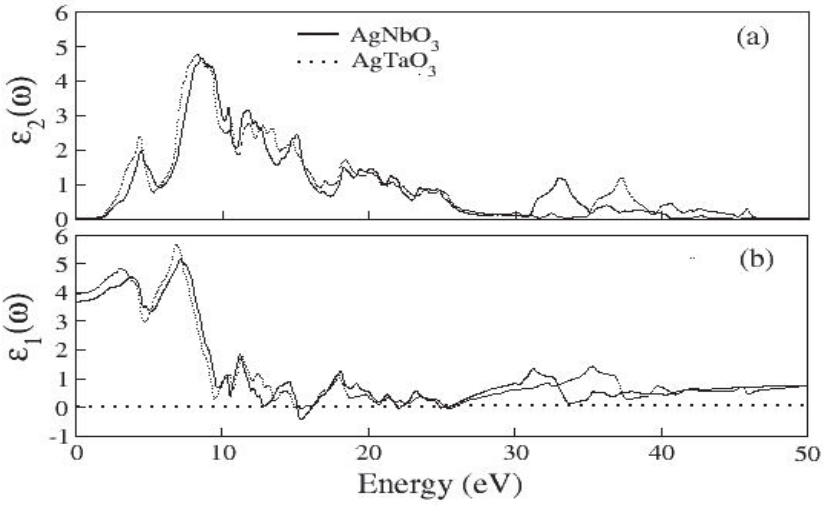

Fig. 6. The calculated (a) imaginary part $\varepsilon_2(\omega)$ and (b) real part $\varepsilon_1(\omega)$ of dielectric function for $AgNbO_3$ and $AgTaO_3$.

The real and imaginary parts of dielectric function lead to the calculations of all other optical parameters such as refractive index, reflectivity, optical conductivity and absorption coefficient of these compounds. The optical response of $AgNbO_3$ and $AgTaO_3$ is investigated by calculating the optical parameters, such as complex dielectric function, refractive index, extinction coefficient, reflectivity and energy loss spectrum, using OPTIC package[33] implanted in WIEN2K.

The real and imaginary parts of dielectric function, $\varepsilon_2(\omega)$ and $\varepsilon_1(\omega)$, for $AgNbO_3$ are shown in Fig. 6. It is clear from the figure that the imaginary part of the dielectric function shows six major peaks at 4.51, 8.69, 11.89, 15.25, 22.55 and 33.13 eV. The highest peak in $\varepsilon_2(\omega)$ at 8.69 eV corresponds to the transition from O $2p$ state to Nb $4d$ state. While, for higher energies some other peaks are observed at 15.25 eV, 22.25 eV and 33.13 eV, which correspond mainly due to the transitions from the semi-core states given in Fig. 6(a). It is also clear from the figure that for $AgTaO_3$, the highest peak of the $\varepsilon_2(\omega)$ curve is at 8.37 eV, which corresponds to transition from O $2p$ state to Ta $5d$ state. Some other peaks are also evident for the compound at 8.77 eV, 22.05 eV and 37.32 eV, which correspond to the transitions from semi-core states, and are shown as dotted line. The first peak energy for $AgNbO_3$ (4.34 eV) is lower than first peak energy for $AgTaO_3$ (4.62 eV). This difference in energy may be attributed mainly due to the difference in the bandgaps of the two materials, because first peak in the plot occurs due the transition from the upper valence band to the lower conduction band

The real parts $\varepsilon_1(\omega)$ of the calculated dielectric function for $AgNbO_3$ and $AgTaO_3$ in cubic phase are shown in Fig. 6(b). First peaks of $\varepsilon_1(\omega)$ for $AgNbO_3$ and $AgTaO_3$ are at energy range 3.01 eV and 3.92 eV, respectively that originate from

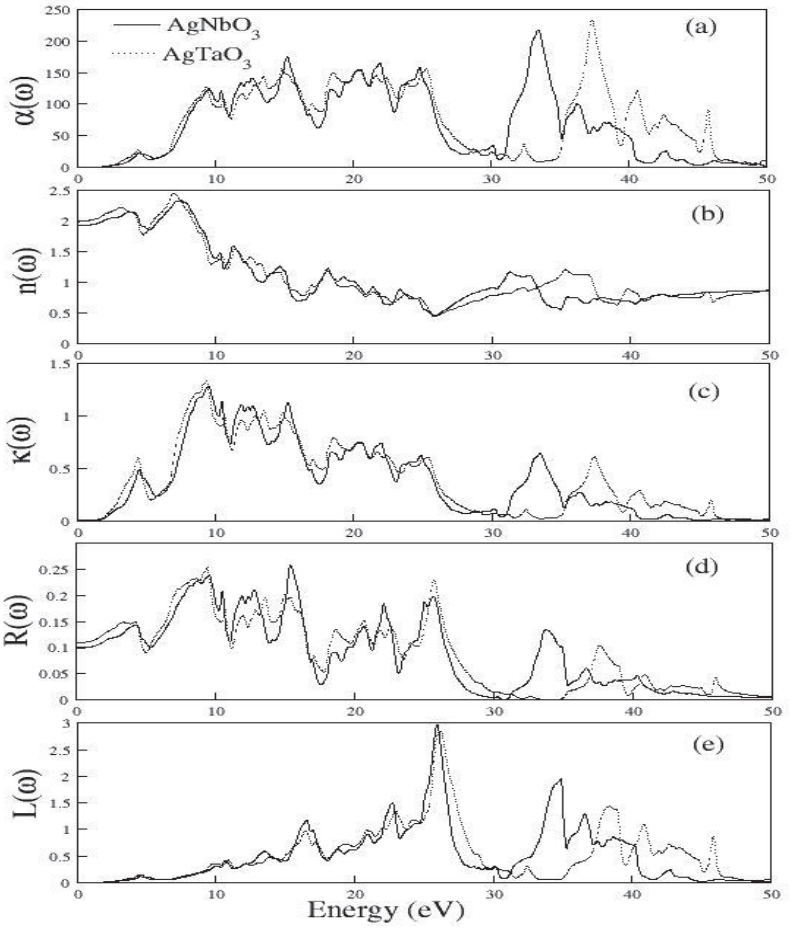

Fig. 7. The calculated optical parameters such as (a) absorption coefficient, (b) refractive index, (c) extinction coefficient, (d) reflectivity and (e) energy-loss spectrum for $AgNbO_3$ and $AgTaO_3$.

O $2p$ state to Nb $4d$ state and O $2p$ state to Ta $5d$ state. As the energy increases, the behavior of peak changes, which reaches a minimum at 9.88 eV for $AgNbO_3$ and 9.63 eV for $AgTaO_3$, respectively. The values of static dielectric constants $\varepsilon_1(0)$ for $AgNbO_3$ and $AgTaO_3$ in cubic phase are 3.89 eV and 4.18 eV, respectively. These values are quite different from those calculated by pseudopotential method.[16]

The energy dependence of absorption coefficient, refractive index, extinction coefficient, reflectivity and energy-loss spectrum for $AgNbO_3$ and $AgTaO_3$ are given in Figs. 7(a)–7(e). These results are derived from the dielectric function. The start of absorption spectra for $AgNbO_3$ and $AgTaO_3$ is at 2.15 eV and 2.98 eV, respectively and these results correspond to indirect transitions in these materials.

The value of the static refractive index $n(0)$ for $AgNbO_3$ is 1.96 and for $AgTaO_3$ is 2.09. It increases with the increase in energy in the transparent region, reaches

to its peak value in the ultraviolet at about 8.05 eV for $AgNbO_3$ and 7.30 eV for $AgTaO_3$ and then decreases to minimum at high energies. The imaginary part of dielectric function and static real part of dielectric function correspond to local maxima of extinction coefficient $k(\omega)$ and is shown in Fig. 7(c).

Electron energy loss function, $L(\omega)$, is a significant factor unfolding the energy loss of a fast electron passing through a material. The main peaks in $L(\omega)$ represent the feature that is associated with plasma resonance and the corresponding frequency known as plasma frequency.[34] These peaks correspond to irregular edges in the reflectivity spectrum, and hence an abrupt reduction occurs at these peak values in the reflectivity spectrum, as shown in Fig. 7(e).

3.4. *Thermoelectric properties*

The transport behavior is investigated using the BoltzTraP code.[36] The calculation of transport properties requires a very dense **k** grid, here, a dense **k**-mesh of $50 \times 50 \times 50$ points is used for the thermoelectric calculations. This approach yields accurate results for various types of TE materials.[37–40] Within BoltzTraP, the constant relaxation time τ is assumed to be a constant with respect to the wave vector **k** and energy around the Fermi level, and the effect of doping is introduced by the rigid band approximation. Within the relaxation-time approximation, the thermo power (Seebeck coefficient (S)) can be obtained directly from the electronic structure without switching parameters.

The efficiency of thermoelectric devices is determined by the dimensionless figure of merit, $zT = \sigma S^2 T/\kappa$, where σ is the electrical conductivity, S is the Seebeck coefficient, T is the temperature, and κ is the thermal conductivity. The latter comprises lattice (κ_{lattice}) and electronic (κ_{electron}) contributions, $\kappa_{\text{total}} = \kappa_{\text{lattice}} + \kappa_{\text{electron}}$. In order to achieve a high efficiency, the thermoelectric material, in general, should be a good electrical and poor thermal conductor and, at the same time, possess a high Seebeck coefficient.

Figure 8 shows the temperature dependence of the thermo power for $AgNbO_3$ and $AgTaO_3$ with p- and n-type carrier concentration at fixed to 10^{19} cm^{-3}. High thermopower S is observed in n-type $AgNbO_3$ over whole temperature range as compared to $AgTaO_3$. Room temperature thermo powers are -375 μV/K and -175 μV/K for n-type $AgNbO_3$ and $AgTaO_3$, respectively. While in p-type both materials posses similar behavior (500 μV/K at 300 K). This value is quite similar to their iso-structural compounds like $SrTiO_3$.

Previously reported perovskites such as $SrTiO_3$, $BaTiO_3$ and $PbTiO_3$ have bandgaps around 3 eV (insulators) which is far from the visible region and Seebeck values are always high for large band gap materials. While at the same time electrical conductivity in very low, which results in low S_σ^2 (Power factor). In our study, case bandgap is around 1.5 eV which half of them and a moderate doping could make these materials as good candidate for optoelectronic and thermoelectric devices.

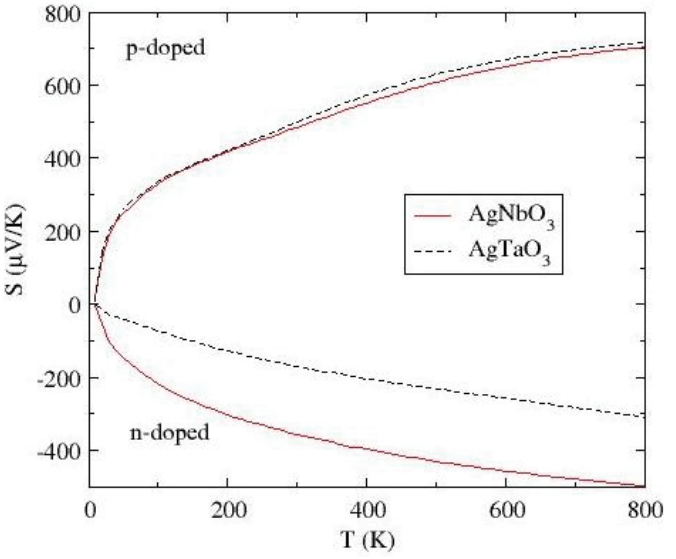

Fig. 8. Thermo power (S) of $AgNbO_3$ and $AgTaO_3$ with respect to temperature under for both p- and n-type doping keeping doping level fixed at 10^{19} cm^{-3}.

4. Conclusion

In this study, FP-LAPW + lo method within the framework of density functional theory has been used to study structural, electronic, optical and thermoelectric properties of $AgMO_3$ (M = V, Nb and Ta) material systems. The calculated structural parameters are in good agreement with the experimental results. The electronic structure calculations show that $AgNbO_3$ and $AgTaO_3$ are indirect bandgap materials while $AgVO_3$ is metallic. Band structures are further used to analyze the interband contribution of the optical response functions. High thermo power -375 μV/K is observed in n-type $AgNbO_3$ as compared to $AgTaO_3$ ($S = -175$ μV/K) at room temperature. It is expected that the present study will provide better insight in understanding electronic as well as thermoelectric properties of these materials.

Acknowledgment

The authors extend their appreciation to the Deanship of Scientific Research at King Saud University for funding the work through the Research Group Project No. RGP–VPP–311.

References

1. W. Fortin, G. E. Kugel and J. Kania, *J. Appl. Phys.* **79** (1996) 4273.
2. F. Zimmermann, W. Menesklou and E. J. Ivers-Tiffee, *J. Eur. Ceram. Soc.* **24** (2004) 1811.

3. G. Li, K. Chao, C. Ye and H. Peng, *Mater. Lett.* **62** (2008) 735.
4. D. Fu, M. Endo, H. Taniguchi, T. Taniyama and M. Itoh, *Appl. Phys. Lett.* **90** (2007) 252907.
5. H. P. Soon, H. Taniguchi and M. Itoh, *Appl. Phys. Lett.* **95** (2009) 242904.
6. J. Y. Kim and A. M. Grishin, *Thin Solid Films* **515** (2006) 615.
7. M. Kruczek, E. Talik and A. Kania, *Solid State Commun.* **137** (2006) 469.
8. A. Kania, *J. Phys. D: Appl. Phys.* **34** (2001) 1447.
9. P. Fleury and R. Kohlmuller, *C. R. Acad. Sci. Paris* **262** (1966) 475.
10. S. Sharma, M. Panthofer, M. Jansen and A. Ramanan, *Mater. Chem. Phys.* **91** (2005) 257.
11. P. Sciau, A. Kania, D. Dkhil, E. Suard and A. Ratuszna, *J. Phys.: Condens. Matter* **16** (2004) 2795.
12. G. E. Kugel, M. D. Fontana, M. Hafid, K. Roleder, A. Kania and M. Pawelczyk, *J. Phys. C* **20** (1987) 1217.
13. A. Ratuszna, J. Pawluk and A. Kania, *Phase Trans.* **7** (2003) 64.
14. I. Grinberga and A. M. Rappe, *Appl. Phys. Lett.* **85** (2004) 1760.
15. J. Sucharicz, A. Kania, G. Stopa and R. Bujakiewicz-Koronska, *Phase Trans.* **80** (2007) 123.
16. S. Cabuk and S. Simsek, *Cent. Eur. J. Phys.* **6** (2008) 730.
17. M. Volant, D. Suvorov, C. Hoffmann and H. Sommoriva, *J. Eur. Ceram. Soc.* **21** (2001) 2647.
18. A. Kania and J. Kwapulinski, *J. Phys.: Condens. Matter* **11** (1999) 8933.
19. S. Cabuk, H. Akkus and A. M. Mamedoc, *Physica B* **394** (2007) 81.
20. P. Bhala, K. Schwarz, G. K. H. Madsen, D. Kvanicka and J. Luitz, *WIEN2K: An Augmented Plane Wave+Local Orbital Program for Calculating Crystal Properties* (Karlheinz Schwarz, Technische Universität, Wien, Austria, 2001), ISBN:3-9501031-1-1-2.
21. B. Amin, R. Khenata, A. Bouhemadou, I. Ahmad and M. Maqbool, *Phys. B: Condens. Matter* **407** (2012) 2588.
22. B. Amin and I. Ahmad, *J. Appl. Phys.* **106** (2009) 093710; Y. Saeed, A. Shaukat, N. Ikram and M. Tanveer, *J. Phys. Chem. Solids* **69** (2009) 1676.
23. B. Amin, S. Arif, I. Ahmad, M. Maqbool, R. Ahmad, S. Goumri-Said and K. Prisbrey, *J. Electron. Mater.* **40** (2011) 1428.
24. T. P. Kaloni, N. Singh and U. Schwingenschlogl, arXiv:1312.7127; T. P. Kaloni, R. Faccio and U. Schwingenschlogl, *Carbon* **64** (2013) 281.
25. T. P. Kaloni and U. Schwingenschlogl, *J. Appl. Phys.* **114** (2013) 184307; T. P. Kaloni, M. Tahir and U. Schwingenschlogl, *Sci. Rep.* **3** (2013) 3192.
26. T. P. Kaloni and A. V. Balatsky, *Eur. Phys. Lett.* **104** (2013) 47013; T. P. Kaloni and U. Schwingenschlogl, *Chem. Phys. Lett.* **583** (2013) 137.
27. T. P. Kaloni and S. Mukherjee, *Mod. Phys. Lett. B* **25** (2011) 1855; T. P. Kaloni, S. Gangopadhyay, N. Singh, B. Jones and U. Schwingenschlogl, *Phys. Rev. B* **88** (2013) 235418.
28. Z. Wu and R. E. Cohen, *Phys. Rev. B* **73** (2006) 235116.
29. F. D. Murnaghan, *Proc. Natl. Acad. Sci. USA* **30** (1994) 244.
30. H. Kato, H. Kobayashi and A. Kudo, *J. Phys. Chem. B* **106** (2002) 12441.
31. M. A. Khan, A. Kashyap, A. K. Solanki, T. Nautiyal and S. Auluck, *Phys. Rev. B* **23** (1993) 16974.
32. F. Wooten, *Optical Properties of Solids* (Academic Press, New York, 1972).
33. C. Ambrosch-Draxl, J. A. Majewski, P. Vogl and G. Leising, *Phys. Rev. B* **51** (1995) 9665.

34. O. L. Anderson, *J. Phys. Chem. Solids* **24** (1963) 909.
35. S. A. Prosandeev, *Phys. Solid State* **47** (2005) 2130.
36. G. K. H. Madsen and D. J. Singh, *Comput. Phys. Commun.* **175** (2006) 67.
37. G. K. H. Madsen, K. Schwarz, P. Blaha and D. J. Singh, *Phys. Rev. B* **68** (2003) 125212.
38. Y. Saeed, N. Singh, D. Parker and U. Schwingenschlogl, *J. Appl. Phys.* **113** (2013) 163706.
39. Y. Saeed, N. Singh and U. Schwingenschlogl, *Adv. Funct. Mater.* **22** (2012) 2792.
40. Y. Saeed, N. Singh and U. Schwingenschlogl, *Appl. Phys. Lett.* **104** (2014) 033105.
41. B. Qiu *et al.*, *Int. J. Mod. Phys. B* **28** (2014) 1450031.